Photoelectron Imaging Spectroscopy for (2+1) Resonance-Enhanced Multiphoton Ionization of Atomic Bromine

Yong Shin Kim,[*] Young-Jae Jung,[†] Weekyung Kang,[‡] and Kyung-Hoon Jung[§]

Micro-Electronics Technology Lab., Electronics and Telecommunications Research Institute, Taejon 305-350, Korea
[†]Samsung Electronics Co., Yongin, Kyunggi-do 449-711, Korea
[‡]Division of Basic Science, Soong Sil University, Seoul 173-763, Korea
[§]Department of Chemistry and School of Molecular Science (BK21), Korea Advanced Institute of Science and Technology, Taejon 305-701, Korea
Received October 5, 2001

Two-photon resonant third photon ionization of atomic bromine ($4p^5\ ^2P_{3/2}$ and $^2P_{1/2}$) has been studied using a photoelectron imaging spectroscopy in the wavelength region 250 - 278 nm. The technique has yielded simultaneously both relative branching ratios to the three levels of Br^+ ($^3P_2$, $^3P_{0,1}$ and $^1D_2$) with $4p^4$ configuration and the angular distributions of outgoing photoelectrons. The product branching ratios reveal a strong propensity to populate particular levels in many cases. Several pathways have been documented for selective formation of $Br^+(^3P_2)$ and $Br^+(^3P_{0,1})$ ions. In general, the final ion level distributions are dominated by the preservation of the ion core configuration of a resonant excited state. Some deviations from this simple picture are discussed in terms of the configuration interaction of resonant states and the autoionization in the continuum. The photoelectron angular distributions are qualitatively similar for all transitions, with a positive A_2 anisotropy coefficient of 1.0 - 2.0 and negligible A_4 in most cases, which suggests that the angular distribution is mainly determined by the single-photon ionization process of a resonant excited state induced from the third photon absorption.

Keywords : Photoelectron spectroscopy, REMPI, Atomic bromide.

Introduction

Photoelectron spectroscopy coupled with the resonance-enhanced multiphoton ionization (REMPI) has proven to be a powerful tool for studying the photoionization dynamics of excited states of neutral atoms. A number of such investigations have been performed on carbon,[1] nitrogen,[2] oxygen,[3] phosphorus,[4] sulfur,[5] transition metals,[6,7] halogen atoms[8,9] and inert gases.[10,11] Kinetic energy and angular distributions of outgoing electrons are important physical quantities in the photoelectron spectroscopy. The kinetic energy distribution provides information about the internal state of the remaining ion core, while the angular distribution includes the partial wave character of outgoing electrons and the alignment of the resonant intermediate state. In conventional photoelectron spectroscopy, the kinetic energy distribution is determined from the flight time measurement of ejected photoelectrons at a fixed angle with respect to the laser polarization direction. The angular distribution is therefore acquired from repeated measurements by rotating either the laser polarization vector or the detector system. To overcome these time-consuming processes, the photoelectron imaging technique has been developed to obtain the kinetic energy and angular distributions simultaneously.[12]

In this work, we report a work on the photoionization of atomic bromine excited by (2 + 1) REMPI in the 250-278 nm region, using the photoelectron imaging technique. The ionization process is depicted as follows:

$$Br\ (^{2S''+1}L''_{J''}) \xrightarrow{2h\nu} Br^*\ (^{2S'+1}L'_{J'}) \xrightarrow{h\nu} Br^+\ (^{2S^++1}L^+_{J^+}) + e \quad (1)$$

where the term symbol notation of initial, excited intermediate and final levels follows the Russell-Saunders (LS) coupling scheme. The double-primed symbols denote the initial state quantum numbers, the single primes the excited intermediate states and the superscript '+' the final state. The odd parity notation has been omitted from the term symbols since all the initial and intermediate states are of odd parity. Atomic bromine is produced in two spin-orbit states, $^2P_{3/2}$ and $^2P_{1/2}$, with $[Ar]4s^24p^5$ ground configuration from ultraviolet photolysis of CF_2Br_2. The ground configuration of ionic bromine is $[Ar]4s^24p^4$ which splits into three terms ^3P, ^1D, and ^1S in ascending order of energy. A schematic diagram of relevant neutral and ionic energy levels is shown in Figure 1. Here we determine the branching ratios among possible ionic levels and their angular distributions with changing an ionization pathway. Most of these results can be understood in frame of the direct ionization of one excited 5*p* electron of resonant excited states with preserving the ion core configuration.

Experimental Section

The photoelectron imaging apparatus used in this study is practically the same as one described elsewhere.[13,14] In order to compensate for the effect of the earth's magnetic field on the photoelectron trajectory, Helmholtz coils were mounted outside the vacuum chamber. A pulsed molecular beam of 1.3% CF_2Br_2 seeded in He was injected into the ionization region through a skimmer. CF_2Br_2 molecules dissociate by the absorption of one UV photon into two channels leading

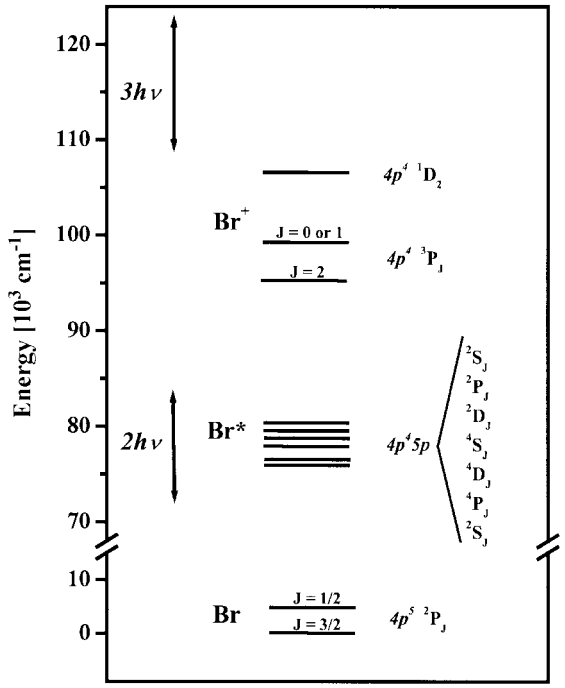

Figure 1. A schematic diagram shows relevant energy levels of neutral and ionic bromine atom. Vertical arrows indicate the two- and three-photon energy regions, respectively, accessed in the present study.

to either a bromine atom of $4p^5\ ^2P_{3/2}$ or $^2P_{1/2}$, together with CF_2Br radical. The bromine atoms were ionized within the same laser pulse *via* two-photon resonance to an intermediate state, plus one-photon ionization. Linearly polarized laser light (250-278 nm) was produced by doubling the output from a nanosecond Nd/YAG-pumped dye laser and was then aligned by a half-wave retardation plate. A photoelectron cloud expanded from the ionization point was projected onto a position-sensitive detector. A CCD camera integrated transient images on a phosphor screen of the position-sensitive detector for several thousand laser shots and the background image, obtained at near non-resonant wavelength, was then subtracted.

Results

Ionic bromine atoms are produced by multiphoton absorption in the wavelength range 250-278 nm from CF_2Br_2. The ion yield spectrum shows very narrow peaks with a typical FWHM of 0.3 cm^{-1}, which implies that the formation of ionic bromine stems from the resonance-enhanced multiphoton ionization of neutral bromine atoms released from the photodissociation of CF_2Br_2. The formation mechanism of bromines can be understood from earlier investigations[15,16] that reported the one-photon excitation ($A \leftarrow X$) followed by prompt dissociation to $CF_2Br + Br$ ($4p^5\ ^2P_{3/2}$ or $^2P_{1/2}$), and two-photon resonant transition plus one-photon ionization of the atomic bromine fragment. Assignments of the intermediate states in (2+1) REMPI are performed for nineteen observed peaks as given in Table 1, and our measured two-photon energies

Table 1. Observed (2+1) REMPI peaks of atomic bromine and their branching ratios among possible ion levels

Wavelength $\lambda_{vac.}$(nm)	Initial level	Intermediate level	Branching ratio (%)		
			$^3P_2$	$^3P_{0,1}$	$^1D_2$
277.68	$5p\ ^2P_{1/2}$	(^{3}P) $5p\ ^4D_{5/2}$	100		
277.23	$5p\ ^2P_{1/2}$	(^{3}P) $5p\ ^4P_{1/2}$	84		16
268.82	$5p\ ^2P_{1/2}$	(^{3}P) $5p\ ^4D_{1/2}$		88	12
267.25	$5p\ ^2P_{1/2}$	(^{3}P) $5p\ ^2D_{5/2}$		100	
266.67	$5p\ ^2P_{1/2}$	(^{3}P) $5p\ ^4S_{3/2}$		100	
266.60	$5p\ ^2P_{3/2}$	(^{3}P) $5p\ ^4P_{3/2}$	100		
264.89	$5p\ ^2P_{1/2}$	(^{3}P) $5p\ ^2P_{3/2}$	5	95	
264.79	$5p\ ^2P_{3/2}$	(^{3}P) $5p\ ^4D_{7/2}$	100		
264.18	$5p\ ^2P_{3/2}$	(^{3}P) $5p\ ^4D_{5/2}$	100		
263.80	$5p\ ^2P_{3/2}$	(^{3}P) $5p\ ^4P_{1/2}$	89		11
263.09	$5p\ ^2P_{1/2}$	(^{3}P) $5p\ ^2D_{3/2}$		100	
262.50	$5p\ ^2P_{1/2}$	(^{3}P) $5p\ ^2S_{1/2}$		77	23
260.57	$5p\ ^2P_{3/2}$	(^{3}P) $5p\ ^4D_{3/2}$	69	15	18
256.12	$5p\ ^2P_{3/2}$	(^{3}P) $5p\ ^4D_{1/2}$		89	11
254.70	$5p\ ^2P_{3/2}$	(^{3}P) $5p\ ^2D_{5/2}$		100	
254.17	$5p\ ^2P_{3/2}$	(^{3}P) $5p\ ^4S_{3/2}$		93	7
252.55	$5p\ ^2P_{3/2}$	(^{3}P) $5p\ ^2P_{3/2}$		100	
250.91	$5p\ ^2P_{3/2}$	(^{3}P) $5p\ ^2D_{3/2}$		92	8
250.37	$5p\ ^2P_{3/2}$	(^{3}P) $5p\ ^2S_{1/2}$		75	25

agree well with literature values.[17] Eight of these arise from the first spin-orbit excited state ($4p^5\ ^2P_{1/2}$) and the rest are from the ground state ($4p^5\ ^2P_{3/2}$).

Two typical raw images of photoelectrons ejected from bromine atoms are illustrated in Figure 2 and show concentric rings. The shape of all the rings is anisotropic and displays the polar-cap appearance characteristic of a near $\cos^2\theta$ angular distribution, where θ is the angle between the direction of the outgoing electron and the laser polarization axis. The number and size of the rings in each image vary with irradiation wavelength of the laser light, *i.e.*, one dominant ring at 264.89 nm (Fig. 2(a)) and three rings at 260.57 (Fig. 2(b)), respectively.

The raw images are the two-dimensional projection of three-dimensional speed and angular distributions of photoelectrons. The three-dimensional distributions are reconstructed by Abel inversion of the raw images since the projection is made perpendicular to the laser polarization direction, around which the spatial distribution of photoelectrons has a cylindrical symmetry. Since Abel transformation is very sensitive to noise, the raw images are presmoothed with the Gaussian filter with a 7×7 window and a standard deviation of 2 pixel units to suppress unwanted artifacts during the transformation. The distance from the center of the reconstructed image is proportional to the speed of an ejected photoelectron. Utilizing the proportionality coefficient determined by experiments, the speed distribution of photoelectrons $P(v)$ is obtained from the angle integration of the reconstructed image as a function of the pixel distance from the center and is readily transformed into kinetic energy distribution $P(E_k)$ by the equation:

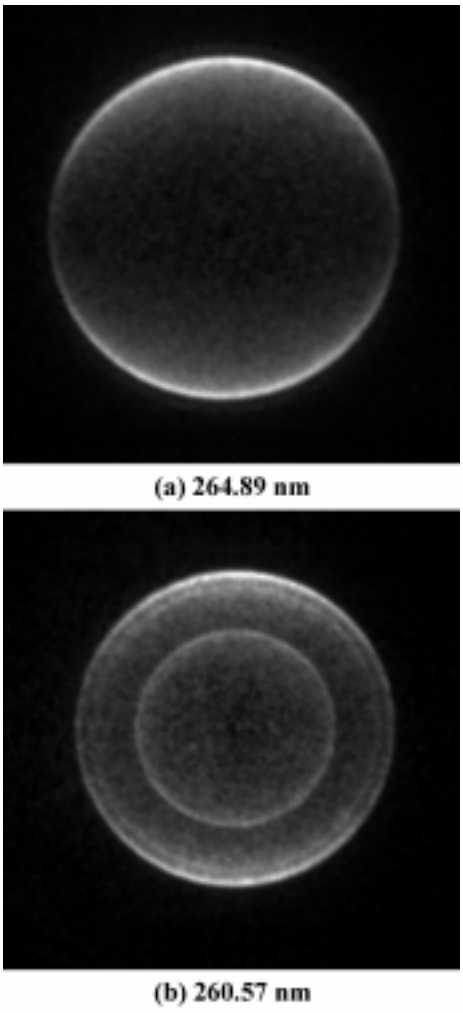

Figure 2. Raw two-dimensional images of photoelectrons ejected from a bromine atom *via* (2+1) REMPI at (a) 264.89 and (b) 260.57 nm. The laser polarization vectors are parallel to the vertical axis and white regions of the black and white images show a higher population of ejected photoelectrons.

$$P(E_k) = P(v)(dv/dE_k) \quad (2)$$

The internal energy distribution of ionic bromines $P(E_i)$ is then calculated from the kinetic energy distribution using the relationship:

$$P(E_i) = 3h\nu + E_o - P(E_k) \quad (3)$$

where $3h\nu$ is the three-photon energy and E_o is the initial energy of atomic bromine produced from the photolysis with respect to the ground level $4p^5\ ^2P_{3/2}$. Figure 3 shows the internal energy distributions obtained from the images of Figure 2, together with the literature values of ion energy levels. Final ion levels are assigned by comparing the peak energies of the internal energy distribution with the reference values. On the other hand, the energy difference between $^3P_1$ and $^3P_0$ ion levels, 701 cm^{-1}, is too small to detect separately within a resolution of our apparatus. The relative branching ratios of possible ion levels can be calculated from the energy distribution $P(E_i)$ as summarized in Table 1. They

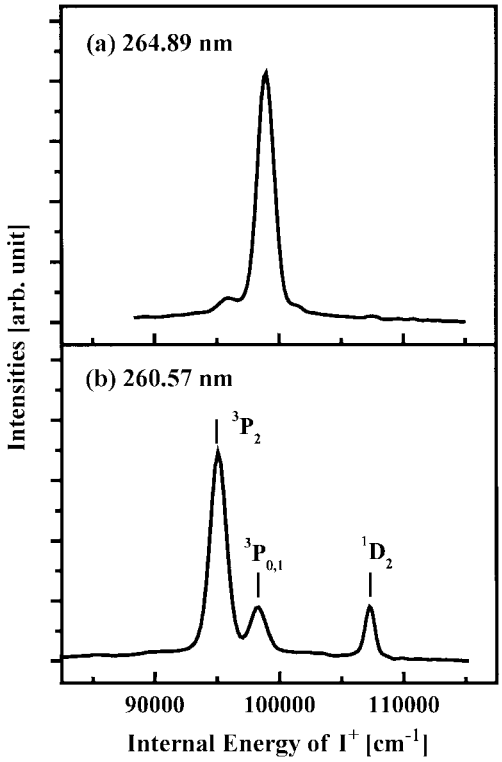

Figure 3. Internal energy distributions of ionic bromine produced by (2+1) REMPI at the two wavelengths of Fig. 2.

clearly demonstrate the level-selective formation of bromine ions. For example, the ion levels of $^3P_2$ and $^3P_{0,1}$ are selectively produced at 277.68 and 267.25 nm, respectively.

A level-selective angular distribution is obtained by the radial integration of the reconstructed image for each ion shell. The angular distribution of photoelectrons, $I(\theta)$, ejected by an REMPI process utilizing single and linearly polarized laser, follows the form: [18,19]

$$I(\theta) \propto \sum_{k=0}^{k_{max}} a_{2k} P_{2k}(\cos\theta) \quad (4)$$

where $P_{2k}(\cos\theta)$ is the Legendre polynomial of order $2k$ and a_{2k} is the anisotropy coefficient. In order to determine the a_{2k} coefficients, the obtained angular distribution is fitted into Eq. 4. All our angular distributions are found to be sufficiently fit with k_{max}=2. Two anisotropy coefficients ($A_2=a_2/a_0$, $A_4=a_4/a_0$) are listed in Tables 2 and 3 for the ground and the first spin-orbit excited state, respectively. Typical angular distributions are displayed in Figure 4. Some general features observed are that the A_2 coefficient gives larger contributions to the spatial anisotropy than the A_4 and its values for the ^3P_J ion states are larger than those of the $^1D_2$.

Discussion

A. Two-photon absorption transition. The two-photon transitions from the $4p^5\ ^2P_{1/2,3/2}$ states of the bromine atom with linearly polarized light are governed by the following selection rules: $\Delta J = J' - J'' = 0, \pm 1, \pm 2$ with $J = 0 \leftarrow /\rightarrow J$

= 1 and $\Delta l = l' - l'' = 0, \pm 2$, where J is the total angular momentum of the whole system and l the orbital angular momentum of a transition electron. The Δl selection rule insures that two-photon excited states will have odd parity due to the odd symmetry of the initial states. In fact, allowed $5p \leftarrow\leftarrow 4p$ transitions accessible with our two-photon energy are only observed in this study. The ΔJ selection rule is also observed in our two-photon transitions. (see Table 1) If the LS coupling scheme were correct, there would be an additional selection rule for the spin conservation, $\Delta S = S' - S'' = 0$. However many spin-changing transitions are also observed for the transition from doublet to quartet state, indicating that the bromine energy levels involved can no longer be described solely by the LS coupling. The violation of the spin selection rule is interpreted as configuration interactions between high lying states with the same values of J' and parity. In the case of an bromine atom, the configuration interaction is found to be substantially stronger than that in P or S atoms,[4,5] which demonstrates the general tendency that the heavier atoms gives the larger the deviation from the LS coupling scheme.

Table 2. Fitted photoelectron angular distribution coefficients for (2 + 1) REMPI of the ground state bromine atom, Br ($4p^5\ ^2P_{3/2}$)

Wavelength $\lambda_{vac.}$ (nm)	Intermediate level	Ion level	Fitted coefficients	
			A_2	A_4
266.60	(^{3}P) 5*p* $^4P_{3/2}$	$^3P_2$	1.52	0.0
264.79	(^{3}P) 5*p* $^4D_{7/2}$	$^3P_2$	1.85	0.8
264.18	(^{3}P) 5*p* $^4D_{5/2}$	$^3P_2$	1.52	0.3
263.80	(^{3}P) 5*p* $^4P_{1/2}$	$^3P_2$	1.38	0.0
		$^1D_2$	0.45	0.1
260.57	(^{3}P) 5*p* $^4D_{3/2}$	$^3P_2$	1.03	0.0
		$^1D_2$	0.27	- 0.1
256.12	(^{3}P) 5*p* $^4D_{1/2}$	$^3P_{0,1}$	1.72	0.3
		$^1D_2$	0.67	0.1
254.70	(^{3}P) 5*p* $^2D_{5/2}$	$^3P_{0,1}$	1.78	0.7
254.17	(^{3}P) 5*p* $^4S_{3/2}$	$^3P_{0,1}$	1.47	0.1
		$^1D_2$	0.79	0.0
252.55	(^{3}P) 5*p* $^2P_{3/2}$	$^3P_{0,1}$	1.65	0.3
250.91	(^{3}P) 5*p* $^2D_{3/2}$	$^3P_{0,1}$	1.63	0.6
		$^1D_2$	0.71	0.2
250.37	(^{3}P) 5*p* $^2S_{1/2}$	$^3P_{0,1}$	1.01	0.2
		$^1D_2$	0.35	0.1

Table 3. Fitted photoelectron angular distribution coefficients for (2+1) REMPI of the first spin-orbit excited state bromine atom, Br ($4p^5\ ^2P_{1/2}$)

Wavelength $\lambda_{vac.}$ (nm)	Intermediate level	Ion level	Fitted coefficients	
			A_2	A_4
277.68	(^{3}P) 5*p* $^4D_{5/2}$	$^3P_2$	1.95	0.7
277.23	(^{3}P) 5*p* $^4P_{1/2}$	$^3P_2$	1.48	0.1
		$^3P_{0,1}$	1.02	- 0.1
268.82	(^{3}P) 5*p* $^4D_{1/2}$	$^3P_{0,1}$	1.44	0.2
		$^1D_2$	0.37	0.2
266.67	(^{3}P) 5*p* $^4S_{3/2}$	$^3P_{0,1}$	1.46	0.5
264.89	(^{3}P) 5*p* $^2P_{3/2}$	$^3P_{0,1}$	1.26	- 0.2
262.50	(^{3}P) 5*p* $^2S_{1/2}$	$^3P_{0,1}$	1.53	0.2
		$^1D_2$	0.60	0.3

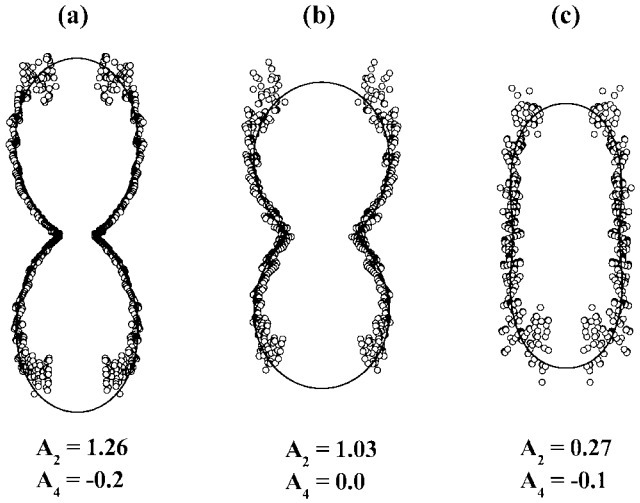

Figure 4. Polar diagrams of the photoelectron angular distributions for (a) $^3P_{0,1}$ ion level via the (^{3}P) 5*p* $^2P_{3/2}$ state, (b) $^3P_2$ and (c) $^1D_2$ levels *via* the (^{3}P) 5*p* $^4D_{3/2}$. The circles show experimental results and the solid lines display least-squares fits using Eq. 4 under the condition of $k_{max} = 2$. The laser polarization vectors are parallel to the vertical axis.

B. Relative branching ratios among final ion levels. The relative branching ratios of possible ion levels are shown as a function of the total energy, $3h\nu + E_o$, in Figure 5. In conventional HeI photoelectron spectroscopy, the branching fractions have been reported to be in fair agreement with their statistical ratios, the relative values of $2J^+ + 1$.[20] However, the statistical ratios depicted by the dotted lines in Figure 5 are found to be different from our results, which generally display favorable production of one level. It implies that the formation of ionic levels should be largely dependent on the ionization pathway, *i.e.*, the electronic structure of resonant excited state. Simply, if an ionization process occurs from an intermediate state by absorbing one photon as our (2+1) REMPI, it may be considered as a conventional one-photon ionization of one electron with no change of the quantum numbers of any other electrons. In the limitation of single-electron direct ionization, the electron configuration of the ion core of the excited intermediate state is preserved during the ionization process. Although the details of our data cannot be interpreted quantitatively, the core-conservation rule allows us to predict the ionization pathway into final ion levels as the starting point. Since the core term of all the intermediate levels corresponds to ^{3}P, the final ion level is therefore predicted to be ^{3}P term under the core-conservation assumption. The core-preserving ionization from resonance-excited states have been documented for many atoms; nonmetals (P, S),[4,5] transition metals (Fe, Ti, V)[6,7] and inert gases (Ar, Kr, Xe).[8,9] Compared with these atoms, an bromine atom has deviated more from the simple picture. It suggests that there is much more possibility of a core-

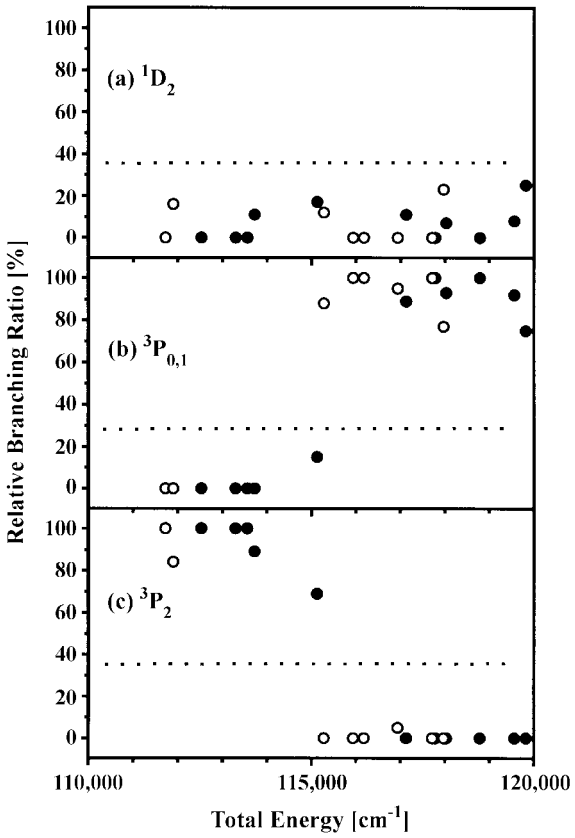

Figure 5. Relative branching ratios for three levels of ionic bromine as a function of the total energy, namely three-photon energy plus internal energy of initial state. Initial states of the hollow symbols are the first excited spin-orbit state of Br $4p^5\ ^2P_{1/2}$ while the filled symbols indicate the initial ground state $4p^5\ ^2P_{3/2}$. The dotted lines show the statistical branching ratios calculated from the $2J^+ + 1$ values of possible ionic levels.

changing ionization pathway as discussed below. Another striking feature in Figure 5 is an abrupt change in the relative population between $^3P_2$ and $^3P_{0,1}$ ion levels as a function of the total excitation energy. The formation of $^3P_{0,1}$ levels is dominant in the energy range from 115000 to 120000 cm^{-1} while the $^3P_2$ level is produced mainly in the 112000-115000 cm^{-1} regions. The core-changing ionization is attributed to several factors including the configuration interaction of the resonance state by other excited states with different ion cores, and the autoionizing resonance in the continuum.

If the same intermediate state is formed from the two different initial states in a one-color experiment, the total energy must differ by half of their spin-orbit energy, 1843 cm^{-1}. Therefore, the comparison of the branching ratios between these two excitation channels provides a chance to evaluate the autoionization effects on the final ion level distribution. We have observed many such transitions for 5*p* $^4D_{5/2}$, 5*p* $^4P_{1/2}$, 5*p* $^4D_{1/2}$, 5*p* $^2D_{5/2}$, 5*p* $^4S_{3/2}$, 5*p* $^2P_{3/2}$ and 5*p* $^2D_{3/2}$ intermediate levels. The possibility of the anisotropic distribution in magnetic subshells resulting from the photodissociation and the two-photon absorption processes can be excluded in the two $J' = 1/2$ states in particular. The branching ratios of the seven cases are found to be almost identical irrespective of the initial states, which suggests that the autoionization does not affect the final ion distribution strongly.

Therefore, it is reasonable that the core-changing ionization is induced by the configuration interaction. This interaction occurs between intermediate levels with the same values of J' and parity, and generally becomes stronger as the energy difference between mixing states goes smaller. The three levels of 5*s* $^2S_{1/2}$, 5*s* $^2D_{3/2}$ and 5*s* $^2D_{5/2}$ are expected to be promising candidates participating in the configuration interaction due to their small energy difference compared with the studied intermediated 5*p* levels. Especially, the strong core-changing tendency at the levels with $J' = 1/2$ in Table 1 suggests that 5*s* $^2S_{1/2}$ state interacts strongly with the $J' = 1/2$ levels of 5*p* intermediate states.

C. Angular distribution of ejected photoelectrons. The maximum order of Legendre polynomial k_{max} in Eq. 4 is limited by $k_{max} = 3$ due to the total number of photons involved in the (2+1) REMPI and can be reduced further by angular momentum constraints. If only one intermediate J' level is populated in an (n+1) REMPI, the k_{max} is given by the largest integer of the smallest among $n + 1$, $J' + 1$, and l_{max}, where l_{max} is the maximum orbital angular momentum of ejected photoelectrons.[21,22] Only $P_2(\cos\theta)$ and $P_4(\cos\theta)$ Legendre terms, namely $k_{max} = 2$, are enough to analyze our angular distributions for all transitions, which implies involvement of the angular momentum constraints. In 5*p* intermediate levels, only the J' restriction cannot explain the observed $k_{max} = 2$ due to the J' values from 1/2 to 7/2. It suggests that higher-order Legendre terms are limited by l_{max}. In the direct single-electron ionization, the character of outgoing electrons from 5*p* states is a mixture of *s* and *d* partial waves due to the parity rule $\Delta l = \pm 1$ and l_{max} is then equal to 2.

In a given spherical symmetry intermediate state ($J' \leq 1/2$), $k_{max} = 1$ is obtained by the constraint $J' + 1$. Therefore, its angular distribution is described by the single anisotropy coefficient A_2, corresponding to the familiar asymmetry parameter β in the conventional single-photon ionization. We have observed six transitions via the $J' = 1/2$ intermediate state and have found their A_4 anisotropy coefficients to be close to zero. For transitions to nonspherical intermediate states ($J' \geq 3/2$), they have two anisotropy coefficients A_2 and A_4. The A_4 coefficient reflects the anisotropic distribution of the intermediate state in a magnetic subshell because only the A_2 coefficient is sufficient to express the angular distribution resulting from the single-photon ionization of an isotropic intermediate state. In general our angular distributions for the core-conserving pathways, the formation of ^3P_J ionic levels, are characterized by a relative high positive A_2 and a relative low A_4. It suggests that the ionization process conserving the ion core configuration can be considered as parallel single-photon ionization of a highly excited state with a weak magnetic anisotropy. On the other hand, the value of A_2 coefficients for the core-changing transitions, the formation of $^1D_2$ ion, ranges from 0.35 to 0.79. The decrease in the A_2 value suggests significant role of electron-ion inter-

actions in single-electron ionization of open-shell atoms. Since the $4p^5\ ^2P_{1/2}$ initial state has spherical symmetry, the A_4 coefficients of transitions from the initial state reflect the intermediate state alignment induced by the two-photon absorption. These alignments are observed and have the following tendency: the larger the J' value is, the stronger the alignment shows. For example, the A_4 coefficients for the two transitions to the highest $J' = 5/2$ level are 0.7 and 1.3, while the others ($J' = 1/2$ or 3/2) range from -0.1 to 0.5. (see Table 3) These results show that optical alignment exists for the transitions to $J' > 1/2$ states and the magnitude increases as J' goes higher.

Acknowledgment. We dedicated this contribution to Prof. K.-H. Jung on the occasion of his 65th birthday. One of authors (W. Kang) was supported by the Korean Research Foundation (BK 21 program), which is gratefully acknowledged.

References

1. Pratt, S. T.; Dehmer, J. L.; Dehmer, P. M. *J. Chem. Phys.* **1985**, *82*, 676.
2. Pratt, S. T.; Dehmer, J. L.; Dehmer, P. M. *Phys. Rev. A* **1987**, *36*, 1702.
3. Kröll, S.; Lundberg, H.; Persson, A.; Svanberg, S. *Phys. Rev. Lett.* **1985**, *55*, 284.
4. Harbol, M. R.; Appling, J. P.; Goren, A. C. *J. Chem. Phys.* **1994**, *101*, 2659.
5. Appling, J. P.; Harbol, M. R.; Edgington, R. A.; Goren, A. C. *J. Chem. Phys.* **1992**, *97*, 4041.
6. Sanders, L.; Sappey, A. D.; Weisshaar, J. C. *J. Chem. Phys*. **1986**, *85*, 6952.
7. Sanders, L.; Hanton, S. D.; Weisshaar, J. C. *J. Chem. Phys*. **1990,** *92*, 3485.
8. Pratt, S. T. *Phys. Rev. A* **1986**, *33*, 1718.
9. Jung, Y.-J.; Kim, Y. S.; Kang, W. K.; Jung, K.-H. *J. Chem. Phys.* **1997**, *107*, 7187.
10. Sato, K.; Achiba, Y.; Kimura, K. *J. Chem. Phys.* **1984**, *80*, 57.
11. Ganz, J.; Lewandowski, B.; Siegel, A.; Bussert, W.; Waibel, H.; Ruf, M. W.; Hotop, H. *J. Phys. B* **1982**, *15*, L485.
12. Helm, H.; Bjerre, N.; Dyer, M. J.; Huestis, D. L.; Saeed, M. *Phys. Rev. Lett.* **1993**, *70*, 3221.
13. Kang, W. K.; Kim, Y. S.; Jung, K.-H. *Chem. Phys. Lett.* **1995**, *224*, 183.
14. Kim, Y. S.; Kang, W. K.; Jung, K.-H. *J. Chem. Phys*. **1996**, *105*, 551.
15. Krajnovich, D.; Zhang, Z.; Butler, L.; Lee, Y. T. *J. Chem. Phys*. **1984**, *88*, 4561.
16. Arepalli, S.; Presser, N.; Robie, D.; Gordon, R. *J. Chem. Phys. Lett.* **1985**, *117*, 64.
17. Moore, C. E. *Atomic Energy Levels*, Natl. Stand. Ref. Data Ser., Natl. Bur. Stand. Cir. 35; U. S. Government Printing Office: Washington, D. C., 1971; Vol. III.
18. Lambropoulos , P. *Adv. At. Mol. Phys.* **1976**, *17*, 87.
19. Strand, M. P.; Hansen, J.; Chien, R.-L.; Berry, R. S. *Chem. Phys. Lett.* **1978**, *59*, 205.
20. Wang, D.; Li, Y.; Li, S.; Zhao, H. *Chem. Phys. Lett*. **1994**, 222, 167.
21. Dixit, S. N.; McKoy, V. *J. Chem. Phys*. **1985**, *82*, 3546.
22. Appling, J. R.; White, M. G.; Kessler, W. J.; Fernandez, R.; Poliakoff, E. D. *J. Chem. Phys*. **1988**, *88*, 2300.